



RESEARCH LETTER

10.1029/2022GL102616

Key Points:

- Waterborne self-potential and electric resistivity tomography are performed to investigate hyporheic exchange in a bedrock-lined stream
- Waterborne self-potential logging provides an indicator of hyporheic exchange by the polarity of the streaming potential
- Electric resistivity tomography enables characterization of hyporheic exchange flow paths

Correspondence to:

S. J. Ikard,
sikard@usgs.gov

Citation:

Ikard, S. J., Carroll, K. C., Rucker, D. F., Adams, R. F., & Brooks, S. C. (2023). Geoelectric characterization of hyporheic exchange flow in the bedrock-lined streambed of East Fork Poplar Creek, Oak Ridge, Tennessee. *Geophysical Research Letters*, 50, e2022GL102616. <https://doi.org/10.1029/2022GL102616>

Received 21 DEC 2022
 Accepted 17 MAR 2023

Author Contributions:

Conceptualization: Scott J. Ikard, Kenneth C. Carroll, Scott C. Brooks
Data curation: Scott J. Ikard
Formal analysis: Scott J. Ikard
Funding acquisition: Kenneth C. Carroll
Investigation: Scott J. Ikard, Kenneth C. Carroll, Ryan F. Adams
Methodology: Scott J. Ikard, Kenneth C. Carroll, Ryan F. Adams, Scott C. Brooks
Project Administration: Scott J. Ikard, Kenneth C. Carroll
Resources: Scott J. Ikard, Kenneth C. Carroll, Scott C. Brooks

© 2023 Oak Ridge National Laboratory, managed by UT-Battelle, LLC and The Authors. This article has been contributed to by U.S. Government employees and their work is in the public domain in the USA.

This is an open access article under the terms of the [Creative Commons Attribution-NonCommercial-NoDerivs License](https://creativecommons.org/licenses/by-nc-nd/4.0/), which permits use and distribution in any medium, provided the original work is properly cited, the use is non-commercial and no modifications or adaptations are made.

Geoelectric Characterization of Hyporheic Exchange Flow in the Bedrock-Lined Streambed of East Fork Poplar Creek, Oak Ridge, Tennessee

Scott J. Ikard¹ , Kenneth C. Carroll² , Dale F. Rucker³ , Ryan F. Adams⁴, and Scott C. Brooks⁵

¹U.S. Geological Survey, Oklahoma-Texas Water Science Center, Austin, TX, USA, ²New Mexico State University, College of Agricultural, Consumer, and Environmental Sciences, Las Cruces, NM, USA, ³hydroGEOPHYSICS, Inc., Tucson, AZ, USA, ⁴U.S. Geological Survey Lower Mississippi Gulf Water Science Center, Nashville, TN, USA, ⁵Oak Ridge National Laboratory, Oak Ridge, TN, USA

Abstract A multimethod geoelectric survey was implemented between January and March 2022 along a 220-m long reach of the bedrock-lined streambed of East Fork Poplar Creek in Oak Ridge, Tennessee to identify locations of surface-water and groundwater exchange and characterize the subsurface flow paths that convey water between the stream and flood plain. A waterborne self-potential (WaSP) survey was completed in January 2022 to measure the electric streaming-potential field in the stream. Electric resistivity tomography (ERT) was performed in March 2022 on the flood plain adjacent to the WaSP survey reach to map the electric resistivity distribution and characterize the hydrogeology and subsurface flow paths that facilitate surface-water and groundwater exchange in the bedrock-lined stream. The combination of WaSP and ERT data support the qualitative interpretation that surface-water and groundwater exchange likely occurs along fractures in outcropping bedrock and along two fault lines that intersect the limestone creek bed.

Plain Language Summary Groundwater flow creates a natural electrical field on the land surface and in streams. Electrical geophysical measurements, measured on the land surface and in streams, measure both the natural electric field attributed to groundwater flow and artificial electric fields that are created by injecting electric current into the Earth. The natural electric field enables scientists to identify locations in bedrock-lined streambeds where surface-water flows into the subsurface, or where groundwater in the subsurface discharges into the stream, and the artificial electric fields enable scientists to create images of the electrical properties of the subsurface hydrogeology. This information enables subsurface flow paths to be mapped and characterized and locations where water enters or exits the stream to be identified with greater accuracy. We use geoelectric measurements at East Fork Poplar Creek, Oak Ridge, Tennessee to identify apparent locations where water may flow between the bedrock-lined streambed and the flood plain.

1. Introduction

Bedrock rivers present a critical knowledge gap with respect to surface-water (SW) and groundwater (GW) exchange processes and hyporheic zone function (Chow et al., 2021; Kennedy, 2017; Oxtobee and Novakowski, 2002, 2003; Tinkler & Wohl, 1998). Previous scientific studies of SW-GW exchange (referred to herein as hyporheic exchange flows) between rivers and flood plain aquifers have focused almost exclusively on alluvial rivers whose streambeds and flood plains are composed of unconsolidated fluvial sediments (Banks et al., 2011; Brunner et al., 2009, 2011, 2017; Chow et al., 2021; Wroblicky et al., 1998); however, conventional hydraulic geometries and exchange-flow processes in alluvial rivers do not exactly apply to bedrock rivers where a substantial portion of the exchange-flow boundary is hydraulically resistive exposed bedrock that may be either faulted and fractured or covered by a thin veneer of highly mobile alluvial sediment (Tinkler & Wohl, 1998). This identified knowledge gap is important to address because of the many correlated impacts the highly variable hyporheic exchange flows have on hyporheic zone function, drainage basin geomorphology, and riparian ecosystem health.

The hyporheic zone is the interface between SW and GW and is typically defined on a discipline-specific basis (Findlay, 1995; Krause et al., 2011; White, 1993), but in general is understood to encapsulate a near-surface region around a stream where subsurface mixing, storage, and exchange of SW and GW occurs (Bencala, 2005; Findlay, 1995; Harvey & Gooseff, 2015; White, 1993). This loose definition, relevant to alluvial rivers, is adopted

Software: Scott J. Ikard
Supervision: Scott J. Ikard, Kenneth C. Carroll
Validation: Scott J. Ikard
Visualization: Scott J. Ikard
Writing – original draft: Scott J. Ikard
Writing – review & editing: Scott J. Ikard

herein and implies that the hyporheic zone in bedrock rivers can include permeable fault planes, fractures and void spaces such as dissolution cavities, in addition to unconsolidated alluvial sediments that may be intermittently dispersed along the flood plain between bedrock outcrops (Cardenas & Gooseff, 2008). Chow et al. (2021) recently showed how closed loops of hyporheic exchange flow were possible at the bedform scale in bedrock rivers, and that fractures connected to the riverbed in addition to hydrodynamic hydraulic head gradients largely controlled the lateral extent of exchange-flow pathways. Similar to alluvial rivers, the hyporheic zone in bedrock rivers directly impacts the biogeochemical functioning of the riparian system through its exerted influence on hyporheic exchange-flow rates, nutrient dynamics of stream-catchment systems, solute mass transport and residence times, mass transport and concentrations of major ions and metals, and biogeochemical reactivity (Bardini et al., 2012; Clark et al., 2019; Krause et al., 2011; Meghdadi and Javar, 2018; Stegen et al., 2018; Trauth et al., 2014).

Mitigating this identified knowledge gap requires the development of novel scientific methods for characterizing and monitoring hyporheic exchange flow processes in bedrock rivers. Geophysical methods have a crucial role to play because (a) the hydrologic processes are dependent upon complex factors such as spatial heterogeneity of the material properties, flow and transport processes that vary over multiple spatial and temporal scales (Boano et al., 2014), and the geomorphology of the streambed (Chow et al., 2021), and (b) characterization methods developed for alluvial rivers generally have limited uses in bedrock rivers. For example, bedrock-lined streambeds prohibit installation of in-stream piezometers, thermistors and thermocouples, and seepage meters, which impedes crucial measurements needed to quantify the spatial and temporal heterogeneity in hyporheic exchange-flow rates, storage, and residence time (Mohamed, Brooks, et al., 2021). Streamflow gaging using acoustic doppler velocimeters, dilution gaging, and hydrologic tracers provide only net changes in streamflow over a gaged reach and do little to characterize exchange-flow paths and hyporheic zone extent.

Heat-tracing methods, used in alluvial rivers since the 1960s, generally have limited uses in bedrock riverbeds with the exception of the use thermal infrared cameras that image the temperature distribution of the stream surface and distributed temperature sensing (DTS) methods used on the riverbed and within the stream (Anderson, 2005; Briggs et al., 2012; Hare et al., 2015; Mamer & Lowry, 2013; McAliley et al., 2022; Mohamed, Gabrielli, et al., 2021; Rosenberry et al., 2016). DTS methods provide near-continuous temperature data on the riverbed or within the SW through time at fine spatial scales of about 1 m over distances of a few kilometers (Rosenberry et al., 2016) and offer a plausible alternative to point-scale heat tracing in bedrock rivers, because SW is strongly affected by diurnal and annual temperature variations whereas GW temperature remains close to the mean annual air temperature. GW is therefore typically warmer than SW in the summer and cooler than SW in the winter (Hare et al., 2015) and temperature anomalies attributed to GW discharge into SW may be detectable at substantial distances downstream from the discharge point (Briggs et al., 2012). However, DTS methods are limited with respect to identifying SW losses in both alluvial and bedrock rivers unless fiber optic cable is buried into the riverbed, because the seepage-loss rates are typically low relative to streamflow and there is little temperature-loss signal at the riverbed and in the stream (Briggs et al., 2012, 2014). Nevertheless, DTS methods have a foreseeable role to play in identifying hyporheic exchange-flow zones that may be limited in aerial extent between 1 m and a few kilometers in bedrock rivers, particularly when integrated with electrical geophysical methods.

Electrical geophysical measurements have demonstrated applicability in alluvial rivers where they are often used for identifying and monitoring locations of hyporheic exchange flow (Acworth & Dasey, 2003; Crook et al., 2008; Nyquist et al., 2008; Singha et al., 2008), delineating spatial scales of exchange (Valois et al., 2018; S. J. Ikard et al., 2018; S. Ikard et al., 2021; S. J. Ikard et al., 2021), monitoring solute transport and redox processes (Fernandez et al., 2019; Ward et al., 2010), and characterizing the flow paths that convey hyporheic exchange flow (P. McLachlan et al., 2017; P. J. McLachlan et al., 2020). The combination of waterborne self-potential (WaSP) logging and electric resistivity tomography (ERT) surveying is particularly well suited to these end goals, and provides a novel approach for mapping surface-hyporheic exchange locations in bedrock-lined streams. Recent research has shown how these methods, when combined, help to better understand the spatial distribution and continuity of hyporheic exchange flow in alluvial rivers (S. J. Ikard et al., 2018; S. Ikard et al., 2021; S. J. Ikard et al., 2021); however, the applications of this combined approach in alluvial rivers are relatively few, and none have currently (2023) been demonstrated in bedrock rivers. The combined multimethod geoelectric approach using WaSP and ERT measurements in conjunction with SW temperature and conductivity logging is therefore extended herein (for the first time) to the bedrock-lined streambed of East

Fork Poplar Creek in Oak Ridge, Tennessee, to identify hyporheic exchange-flow locations, and to characterize the spatial scales of exchange and the subsurface flow paths that convey water between the stream and the floodplain.

2. Site Description

East Fork Poplar Creek (East Fork) is a third-order, shallow, limestone bedrock-lined stream in the Valley and Ridge physiographic province of the southern Appalachian Mountains in Oak Ridge, Tennessee (Rucker et al., 2021) (Figure 1). East Fork is perennial and flows from its headwaters at the United States Department of Energy's Y-12 National Security Complex (Y12-NSC) for approximately 25 km to its confluence with Poplar Creek. Flow in East Fork originates from springs, GW contributions from the flood plain, storm-water runoff, and the discharge of wastewater in the headwaters at Y12-NSC (Brooks et al., 2017). East Fork is flashy at times, resulting in frequent shifts and changes in stream bedforms and riffles (Loar et al., 2011).

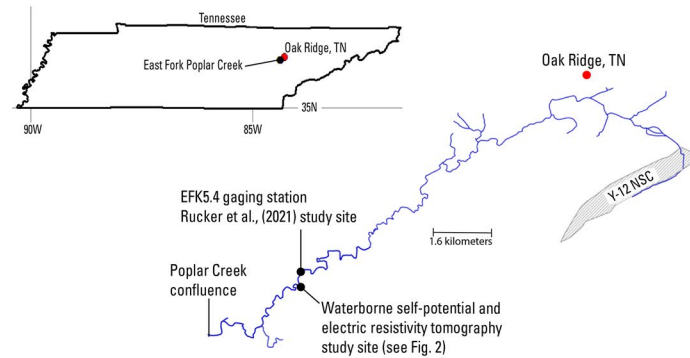
The flood plain and streambed sediments and the surface water in East Fork are contaminated with mercury from historical discharges at the headwaters (Brooks & Southworth, 2011). Remedial actions of the past 25 years have substantially decreased mercury loading into the stream even though the flood plain and streambed sediments continue to store high levels of residual mercury. Low levels of mercury continue to be released from the flood plain into the SW (Loar et al., 2011) where the counteracting processes of methylation into monomethyl mercury, and demethylation of monomethyl mercury into inorganic mercury, are actively occurring (Dong et al., 2010; Rucker et al., 2021). Recent sampling indicated the water within the hyporheic zone of the streambed and flood plain may be an important secondary source of mercury loading into the stream (Demers et al., 2018; Peterson et al., 2018; Rucker et al., 2021), exacerbating the need for an improved understanding of hyporheic zone processes, surface-water and groundwater exchange locations, spatial scales, and flow path characterization for informing future remediation efforts.

The hydrogeology along the survey reach is consistent with the hydrogeology along the nearby EFK5.4 reach that was mapped by Rucker et al. (2021) using ERT (Figure 1a). The flood plain is composed of porous, electrically conductive cobble and gravel covered completely by silt, sand, and small gravel (Rucker et al., 2021), on top of electrically-resistive limestone bedrock of the middle Ordovician Chickamauga Group, which is a thick sequence of shallow-water marine platform carbonate deposits in the northwest part of the Valley and Ridge physiographic province (Ruppel and Walker, 1984). Bedrock outcrops are distributed intermittently along the entire length of the stream (Figure 1c), and the streambed is lined with fractured limestone bedrock that is covered by a thin veneer of porous alluvial sediments in some locations that is highly mobile in the stream (Rucker et al., 2021). SW-GW exchanges between the stream and flood plain are thought to occur predominantly as lateral hyporheic exchange flow through the flood plain and along fracture planes through the limestone bedrock outcrops and streambed (Mohamed, Brooks, et al., 2021). Water-level measurements in flood plain piezometers installed along the EFK5.4 reach in 2012 indicated that the stream was likely gaining at the time of measurement because water-level altitudes measured in flood plain piezometers were slightly higher than the water-level altitude in the stream such that the hydraulic gradient decreased toward the stream (Mohamed, Brooks, et al., 2021; Rucker et al., 2021).

3. Methods

A geoelectric survey combining WaSP logging in the stream and ERT on the adjacent east and west flood plains was completed between January and March 2022 on the East Fork to locate areas of apparent hyporheic exchange between the stream and its flood plain. The survey was located just downstream from the EFK5.4 survey site studied and characterized by Rucker et al. (2021) (Figure 1). The WaSP component of the geoelectric survey was completed on 13 January 2022, and the ERT survey was completed March 6–10, 2022. The WaSP survey reach is shown in Figure 1d (black line) in relation to the locations of ERT profiles ERT0–ERT3 on the flood plain (red lines). Numbered blue crosses correspond to the locations of electrodes used for ERT data acquisition. Waterborne self-potential and ERT surveying methodologies and data processing procedures are illustrated and described in detail by S. J. Ikard et al. (2018), S. Ikard et al. (2021); S. J. Ikard et al. (2021), and Rucker et al. (2021). The WaSP data presented herein and corresponding data processing codes, in addition to inversion parameter settings, formatted input files, and inverted resistivity models corresponding to each ERT line, are included in the corresponding data release (S. J. Ikard et al., 2022).

a. Location Maps of the Waterborne Self-potential and Electric Resistivity Tomography Surveys



b. Photograph of WaSP Survey at the Study Site



c. Photograph of Outcrop Geology along the Survey Reach



d. Map of the Layout of the Geoelectric Survey at East Fork Poplar Creek

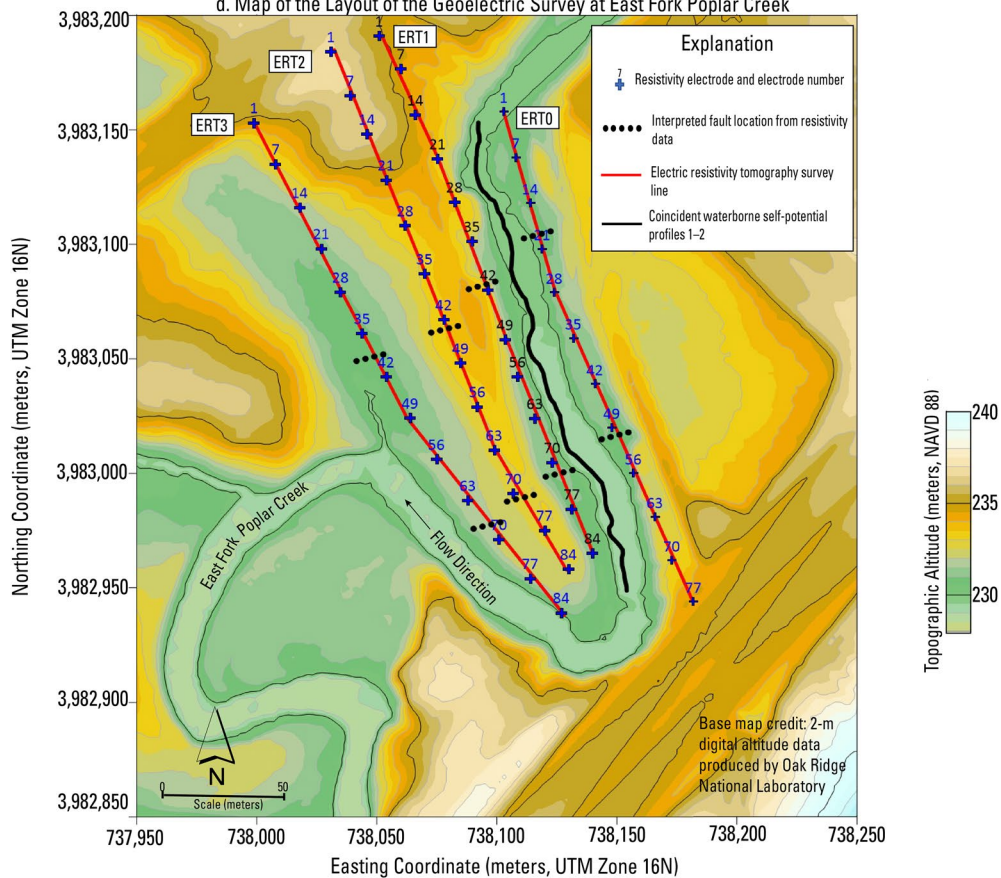


Figure 1.

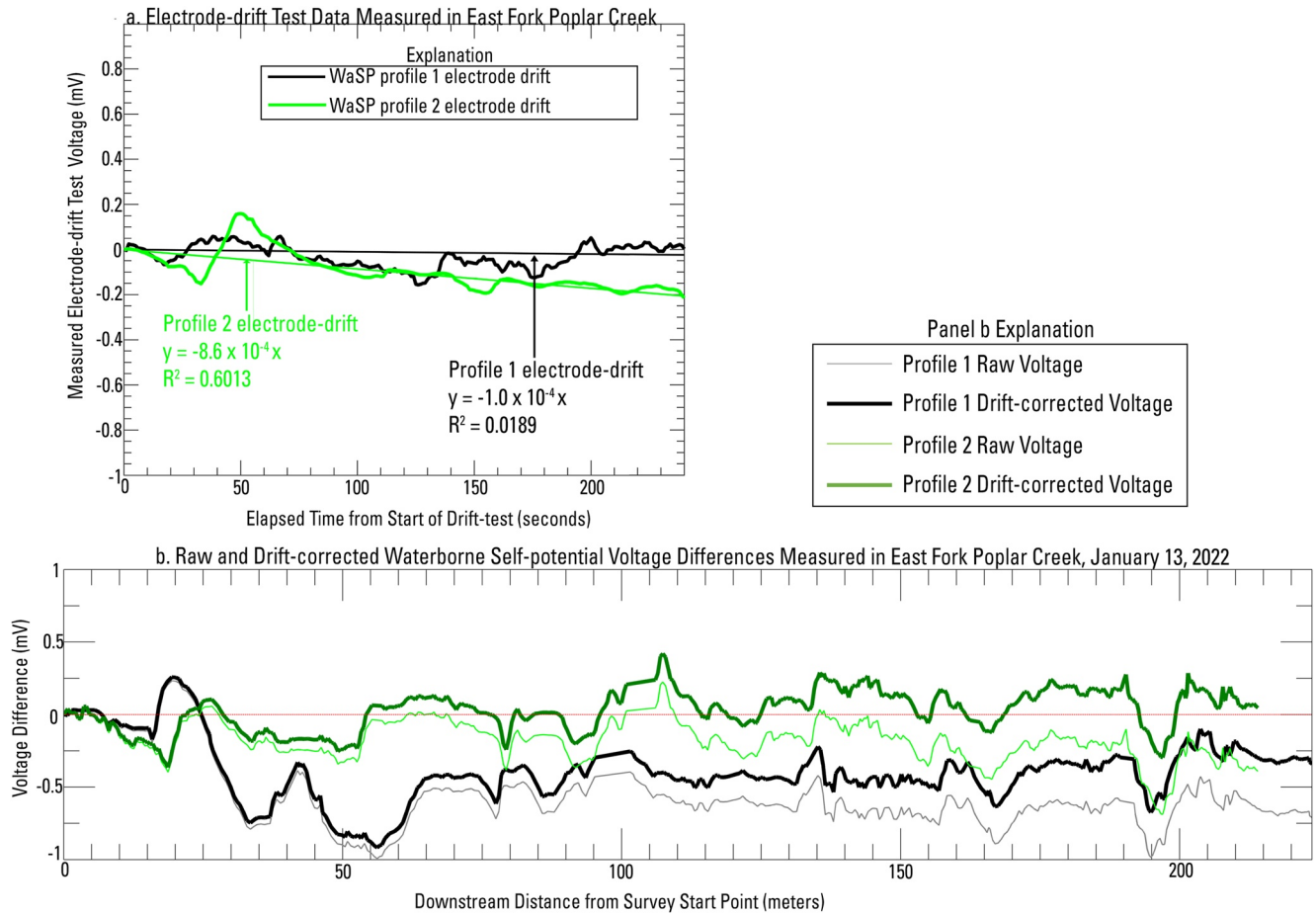


Figure 2. Waterborne self-potential (WaSP) data measured in East Fork Poplar Creek, Oak Ridge, Tennessee, January 2022. (a) Electrode-drift test voltage differences measured in an eddy on the east bank of East Fork Poplar Creek at the upgradient end of the WaSP survey profiles. (b) Raw and drift-corrected waterborne self-potential voltages measured in East Fork Poplar Creek along the west bank. Raw data are shown by the thin curves for each WaSP profile, and drift-corrected data are shown by the bold curves.

3.1. Waterborne Self-Potential Survey

Two repeated WaSP surveys were performed in the stream along the west bank of the survey reach shown in Figure 1d. During each WaSP survey, voltage differences were measured in the stream with an Agilent Technologies U1252 B data-logging multimeter and a 0.6-m long electric dipole comprised of two copper-sulfate electrodes that were suspended approximately 15 cm into the SW beneath a kayak. SW temperature and conductivity data (not shown herein; the data are available online by S. J. Ikard et al. (2022)) were continuously measured with an Onset HOBO conductivity and temperature logger that was also suspended 15 cm beneath the water surface. Electrode-drift tests were performed prior to beginning WaSP data acquisition along each profile and consisted of: (a) allowing the electrodes to equilibrate and stabilize in the surface water for approximately 30 min at the beginning of the survey, (b) positioning the kayak and the WaSP electrodes in the eddy on the east bank at the upgradient end of the survey reach, and (c) measuring voltage differences between electrodes for 240 s while the kayak remained stationary in the eddy. The duration of the electrode-drift tests were held comparable to the duration of the data acquisition along each profile (~300–500 s per profile) to estimate the short-term drift characteristics and apply drift corrections to the WaSP data. The electrode-drift test data are plotted in Figure 2a

Figure 1. Location maps and photographs of the waterborne self-potential survey of East Fork Poplar Creek. (a) Geographic and reach-scale location maps of the survey area. (b) Photograph of the WaSP survey data acquisition. Photograph by Ryan Adams, U.S. Geological Survey. (c) Photograph of limestone bedrock outcrop along the west bank of the survey reach. Photograph by Ryan Adams, U.S. Geological Survey. (d) Map of the layout of the geoelectric survey at East Fork Poplar Creek showing waterborne self-potential survey profiles in the stream and electric resistivity tomography survey lines on the east and west flood plains. UTM: Universal Transverse Mercator. NAVD 88: North American Vertical Datum 1988.

with the electrode drift, which was equal to the slope of the line fitted to the electrode-drift data by ordinary least squares linear regression. The observed electrode-drift rates for WaSP data acquired along survey profiles 1 and 2 were -1×10^{-4} and -8.6×10^{-4} mV/s, respectively; however, the drift rates for each test are comparable for the majority of the duration of drift tests and therefore an electrode drift of -8.6×10^{-4} mV per second was assumed constant during the survey.

The raw voltage-differences measured during the WaSP survey are shown in Figure 2b by the gray and light-green curves, corresponding to profiles 1–2 along the west bank, respectively. The raw voltage differences were corrected for transient electrode drift by subtracting a drift voltage (ΔV_d ; mV) computed from ordinary least squares linear regression lines (Figure 2a) fitted to the electrode-drift test data (ΔV ; mV). A drift voltage corresponding to each WaSP measurement was calculated as $\Delta V_d = -8.6 \times 10^{-4} t$, where t is the elapsed time (seconds) between the beginning of data acquisition on the profile and a given measurement, and the slope of the linear regression line is the electrode-drift rate, equal to -8.6×10^{-4} mV/second. The electrode-drift correction was applied to the raw data in Figure 2 by $\Delta V_c = \Delta V - \Delta V_d$, where ΔV_c (mV, Figure 2b bolded black and green curves) represents the drift-corrected WaSP voltages for profiles 1 and 2, respectively. The drift-corrected data were further processed into electric potential by manually removing apparent electrical noise from the drift-corrected data, calculating the electric field intensity, partitioning the electric-field-intensity data into low and high-spatial frequency components by digital signal processing, and subsequent numerical integration of the high spatial frequency component of the electric field intensity into electrical-potential (S. J. Ikard et al., 2018).

3.2. Electric Resistivity Tomography Survey

Electric resistivity tomography data were measured on 6–10 March 2022 along four survey lines on the east and west flood plains oriented adjacent and approximately parallel to the coincident WaSP profiles measured along the west bank of the stream (Figure 1d). ERT0 on the east flood plain was 228-m long and used 77 stainless steel electrodes separated by 3-m intervals, whereas ERT1–3 on the west flood plain were each 249-m long and used 84 stainless steel electrodes separated by 3-m intervals. The ERT data were measured with an Advanced Geosciences, Incorporated SuperSting R8 resistivity meter with accompanying 56-electrode and 28-electrode switch boxes using the standard Wenner electrode array configuration (Zhody et al., 1974) augmented by gradient array measurements (Cubbage et al., 2017; Rucker et al., 2021). The resistance measurements acquired during each individual ERT acquisition were filtered to remove anomalous noisy measurements (e.g., negative resistance values or values with large associated errors greater than 3% for repeated measurements), and subsequently inverse modeled in the RES2DINVx64 v4.06.23 software (Loke et al., 2013). Inversion was performed using a least squares optimization procedure and a finite element forward operation based on Dey and Morrison (1979) to account for the topography of the ERT lines and obtain an inverted 2D resistivity model of the subsurface beneath each ERT line. Inverse models were iteratively changed from a homogeneous half-space model initial condition until the calculated resistance of the model closely matched that of the measured resistances within an acceptable error tolerance. Additionally, the inversion procedure incorporated spatial-weighting and roughness filters (Loke et al., 2003; Loke et al., 2013) to dampen the effects of noisy resistance measurements and calculate models of the subsurface distribution of electric resistivity beneath the ERT survey lines.

4. Results and Discussion

The WaSP electric-potential profiles are shown in Figure 3 in relation to the inverted resistivity tomograms corresponding to the ERT survey profiles ERT0–1. The electric-potential profile data in Figure 3b appear to be generally repeatable between the two profiles, providing a degree of confidence in the measurements. Repeatable data are most apparent near the downstream end at profile distances greater than about 150 m, although consistent spatial patterns are evident throughout the full length of the profiles. There are some notable differences between the two electric-potential profiles as well, and one example is the transient change between electric-potential profiles 1 and 2 that is evident between about 15 and 50 m from the upstream survey starting point. For example, the electric-potential along profile 1 shows two successive peaks between 15 and 50 m distance that align spatially with the bedrock outcrop shown in Figure 1c, which is annotated on the tomogram corresponding to ERT1 (Figure 3c). The same general pattern is observed in the electric potential data along profile 2; however, the two positive peaks observed in the profile 1 data are smeared into a single relative electric-potential peak and

Comparison of Waterborne Self-potential (WaSP) Data Measured in East Fork Poplar Creek with Electric Resistivity Tomography on the East and West Floodplain

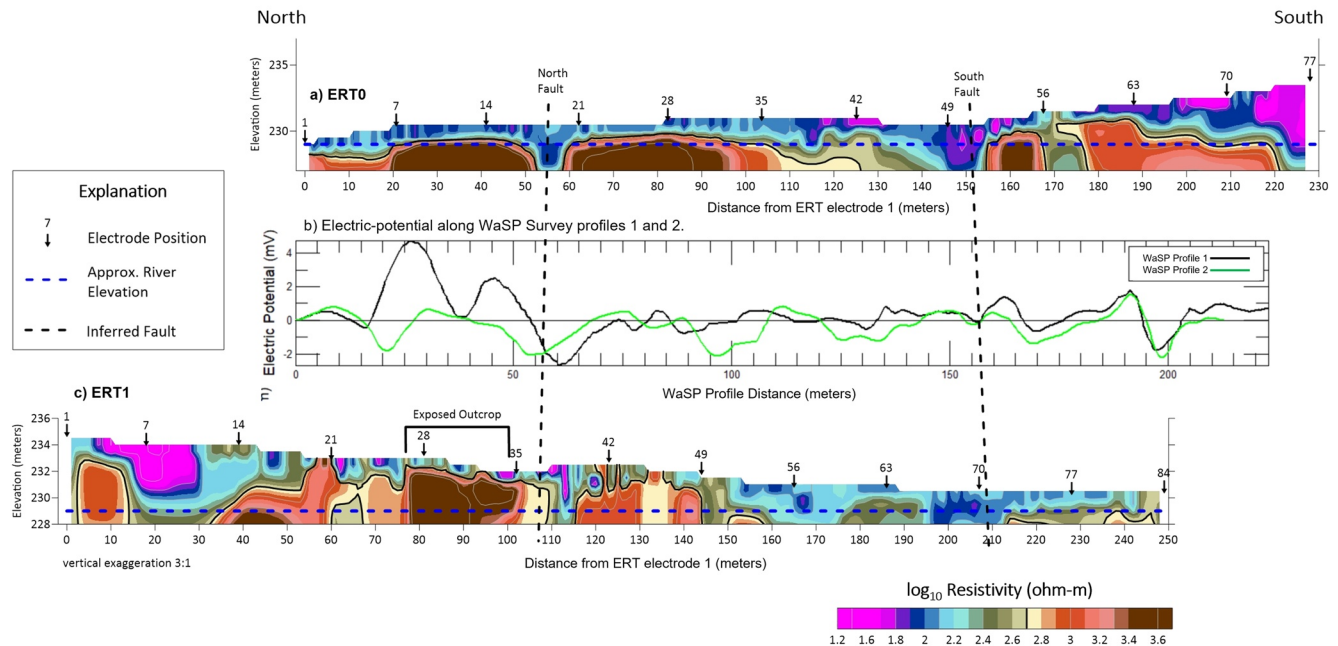


Figure 3. Resistivity tomograms corresponding to survey lines ERT0–ERT1 in comparison to electric-potential profile data along coincident waterborne self-potential profiles 1–2.

therefore noncoherent, and the amplitude of the profile 2 data between 30 and 50 m is attenuated relative to the amplitude of the profile 1 data.

Resistivity tomograms corresponding to ERT survey lines ERT0 and ERT1 on the east and west flood plain, respectively, are shown in Figures 3a and 3c in comparison to the coincident WaSP profiles 1 and 2 measured in the stream parallel to the west bank. The water-level elevation in the stream is annotated in Figures 3a and 3c by the horizontal dashed blue line. Electric resistivity tomography data show \log_{10} transformed values of resistivity in the range of about 1.6–3.981 $\Omega\text{-m}$ as well as some general spatial correlation between the resistivity distributions beneath ERT0–ERT1 and the electric-potential profiles along the west bank of East Fork. Brown shades characterize resistivity values greater than about 2,500 up to a maximum value of about 3,981 $\Omega\text{-m}$ and represent the limestone bedrock observed in outcrop and pictured in Figure 1c and annotated on the tomogram corresponding to ERT1 on the west flood plain. Soil and sediment deposits above the bedrock, characterized by purple and blue shades and representing resistivity in the range of about 15–300 $\Omega\text{-m}$, correspond to porous electrically conductive cobble and gravel covered by silt, sand, and small gravel. Two fault lines are interpreted from the ERT data in Figure 3 and are shown to intersect the WaSP survey reach by comparison of the resistivity distribution on the east and west flood plain. The locations of the inferred fault lines, annotated as north and south faults, are shown in the ERT tomograms by the vertical and near-vertical dashed black lines near WaSP profile distances of about 57 and 157 m and are shown in map-view in Figure 1d relative to the locations of the ERT lines by the horizontal dashed black lines. The north fault is collocated in space with a relative electric-potential decrease and polarity reversal from positive polarity at the bedrock outcrop to negative polarity across the fault, whereas the south fault line appears to be spatially collocated with a relative increase in the electric-potential profile data in WaSP survey profiles 1 and 2. The relative changes in the electric potential profile in the vicinity of the fault lines are interpreted as indicators of apparent hyporheic exchange occurring near the north and south fault lines, respectively based on the field studies and numerical modeling experiments of Valois et al. (2018), S. J. Ikard et al. (2018), S. Ikard et al. (2021), and S. J. Ikard et al. (2021), such that the polarity reversal of the electric-potential data near the north fault line is interpreted as a switch from gaining conditions at the exposed fractured bedrock outcrop to losing-stream conditions across the fault, and the relative electric-potential increase near the south fault is interpreted as an indicator of SW gains if the source of the electric-potential is indeed streaming potential as assumed. It is not entirely clear if the positive peaks in the WaSP profile 1 electric-potential data are attributed to the presence of the resistive bedrock outcrop and related to the large resistivity contrast between the limestone

bedrock and the surrounding alluvial flood plain sediments; however, the entire length of the streambed along the survey reach is lined with resistive bedrock. The relative negative electric-potential anomaly between the anomalous positive electric-potential peaks associated with the bedrock outcrop at WaSP survey distances between 35 and 40 m may potentially indicate a SW loss along a fracture plane in the outcrop. The latter condition is more consistent with the reversal to negative polarity across the north fault just downstream from the bedrock outcrop; however, there are no positive electric-potential anomalies of comparable amplitude collocated with the highly resistive limestone bedrock shown in ERT0 just downstream from the north fault (Figure 3a between profile distances of 60 and 95 m).

In the East Fork, discharge through bedrock fractures is not ubiquitous and may be buried or covered by alluvial, unconsolidated sediment in the streambed. Lateral hyporheic exchange may occur through the thin veneer of unconsolidated streambed sediment (when present) or through lateral exchange with GW in flood plain sediments overlying the bedrock. This is evident in the resistivity contrast between the interpreted north and south faults and the bedrock outcrop annotated in ERT1, which correspond to log-10 transformed resistivity values of less about 300 Ω -m and greater than about 2,500 Ω -m, respectively. The large resistivity contrast between the north and south faults and the limestone bedrock indicates that hyporheic exchange flow paths conveyed along the north and south faults are predominantly through permeable alluvial sediment compared to exchange flow through fractures in the vicinity of the bedrock outcrop.

WaSP surveying has its strengths and limitations like all hydrologic and geophysical methods considered in this paper in regard to their applicability in bedrock rivers. The predominant limitations associated with WaSP measurements are: (a) there are a multitude of physical sources of electric-potential in the riverbed and stream (Nyquist and Corry, 2002) in addition to anthropogenic and natural electrical noise. Interpretations are therefore only apparent until the data are modeled and the uncertainty in the interpretations can be assessed, particularly when auxiliary hydrologic and geophysical data are unavailable to constrain interpretations. Measurements can be especially challenging to interpret without ERT data as the near-surface resistivity distribution will elucidate potential hyporheic exchange flow pathways and also affect the electric-potential field in the stream. With regards to foreseeable and demonstrated strengths, WaSP surveys can provide spatially continuous profiles of electric potential over great distances in both alluvial and bedrock rivers, and when combined with land-based or waterborne ERT, distributed SW temperature and conductivity sensing, and auxiliary hydraulic measurements, WaSP data have demonstrated the potential to resolve SW gain and loss at localized point scales of one m or less (S. J. Ikard et al., 2021), meander bend scales of a few hundred meters (S. J. Ikard et al., 2018), and basin-scales of tens to greater than 100 km (S. J. Ikard et al., 2021; S. J. Ikard et al., 2021; S. J. Ikard & Sparks, 2020). Additional improvements to the WaSP surveying methodology are forthcoming and include integration of bathymetric profiles and profiles of water-quality parameters including turbidity, percent hydrogen, dissolved oxygen, and nitrate and chloride concentrations for improving upon characterization methodologies relevant to hyporheic exchange flows and hyporheic zone function in bedrock rivers.

5. Conclusions

A geoelectric survey combining WaSP logging and ERT was performed along a ~220-m long reach of East Fork Poplar Creek in Oak Ridge, TN to map apparent hyporheic exchange locations between the bedrock-lined streambed and adjacent flood plain. Electric-potential profiles calculated from the WaSP survey data showed conspicuous increases and peak positive anomalies that were spatially aligned with a bedrock outcrop along the survey reach, in addition to a reversal of polarity near the mapped north fault, and a localized increase near the mapped south fault. The combination of WaSP and ERT data support the qualitative interpretation that hyporheic exchange flows occurring between the stream and adjacent flood plain along the survey reach likely occur along fractures in outcropping bedrock and the limestone streambed, as well as along the two permeable faults that intersect the stream. This investigation has developed a geophysical approach combining WaSP and ERT surveying that can be used to map hyporheic exchange flow locations in bedrock rivers with intermittent unconsolidated sediment distributed along fractured bedrock outcrops lining the streambed and used in a complimentary manner to characterize the hyporheic exchange flow paths, which were depicted by the geophysical data to be a complex heterogeneous network of fractures and faults in the limestone bedrock-lined streambed and adjacent flood plain of East Fork Poplar Creek. Noninvasive and repeatable geophysical characterization methods such as this combination of ERT with WaSP may also be a valuable tool for low-cost time-lapse monitoring of changes

in the locations of hyporheic exchange flow in bedrock rivers such as East Fork Poplar Creek where floods alter the spatial distribution of unconsolidated sediment on the streambed each year and change the spatial distribution of hyporheic exchange flows through time.

Data Availability Statement

The waterborne self-potential data, surface-water temperature and conductivity data and corresponding data processing codes, in addition to inversion parameter settings, formatted input files, and inverted resistivity models corresponding to each electric resistivity tomography survey line, are available online as a U.S. Geological Survey data release at <https://doi.org/10.5066/P9BAW75G>.

Acknowledgments

This work was supported by Department of Energy Minority Serving Institution Partnership Program (MSIPP) managed by the Savannah River National Laboratory under BSRA contract TOA 0000525176. Oak Ridge National Laboratory is managed by UT-Battelle, LLC, for the U.S. Department of Energy under contract DE-AC05-00OR22725. This work was partially supported by funding from the U.S. Department of Energy, Office of Science, Biological and Environmental Research, Environmental System Science Program, and is a product of the Science Focus Area (SFA) at Oak Ridge National Laboratory. The authors wish to thank Dr. Martin Briggs for an insightful discussion of heat tracing methods, and Dr. Jesus D. Gomez-Velez, graduate student Yingqiang Xu, and post-doctoral researchers Dr. Chao Wang and Dr. Gabriel Perez for their assistance with data-collection in the field. Additionally, the authors wish to thank the peer-reviewers for assistance in improving this research letter. Any use of trade, firm, or product names is for descriptive purposes only and does not imply endorsement by the U.S. Government. Writings prepared by U.S. Government employees as part of their official duties, including this paper, cannot be copyrighted and are in the public domain.

References

- Acworth, R. I., & Dasey, G. R. (2003). Mapping of the hyporheic zone around a tidal creek using a combination of borehole logging, borehole electrical tomography and cross-creek electrical imaging, New South Wales, Australia. *Hydrogeology Journal*, *11*(3), 368–377. <https://doi.org/10.1007/s10040-003-0258-4>
- Anderson, M. P. (2005). Heat as a ground water tracer. *Ground Water*, *43*(6), 951–968. <https://doi.org/10.1111/j.1745-6584.2005.00052.x>
- Banks, E. W., Simmons, C. T., Love, A. J., & Shand, P. (2011). Assessing spatial and temporal connectivity between surface water and groundwater in a regional catchment: Implications for regional scale water quantity and quality. *Journal of Hydrology*, *404*(1–2), 30–49. <https://doi.org/10.1016/j.jhydrol.2011.04.017>
- Bardini, L., Boano, F., Cardenas, M. B., Revelli, R., & Ridolfi, L. (2012). Nutrient cycling in bedform induced hyporheic zones. *Geochimica et Cosmochimica Acta*, *84*, 47–61. <https://doi.org/10.1016/j.gca.2012.01.025>
- Bencala, K. E. (2005). Hyporheic exchange flows. In M. G. Anderson & J. J. McDonnell (Eds.), *Encyclopedia of hydrological sciences*. John Wiley & Sons, Ltd. <https://doi.org/10.1002/0470848944.hsa126>
- Boano, F., Harvey, J. W., Marion, A., Packman, A. I., Revelli, R., Ridolfi, L., & Wörman, A. (2014). Hyporheic flow and transport processes: Mechanisms, models, and biogeochemical implications. *Reviews of Geophysics*, *52*(4), 603–679. <https://doi.org/10.1002/2012RG000417>
- Briggs, M. A., Lautz, L. K., Buckley, S. F., & Lane, J. W. (2014). Practical limitations on the use of diurnal temperature signals to quantify groundwater upwelling. *Journal of Hydrology*, *519*, 1739–1751. <https://doi.org/10.1016/j.jhydrol.2014.09.030>
- Briggs, M. A., Lautz, L. K., & McKenzie, J. M. (2012). A comparison of fiber-optic distributed temperature sensing to traditional methods of evaluating groundwater inflow to streams. *Hydrological Processes*, *26*(9), 1277–1290. <https://doi.org/10.1002/hyp.8200>
- Brooks, S. C., Eller, V., Dickson, J., Earles, J., Lowe, K., Mehlhorn, T., et al. (2017). *Mercury content of sediments in East Fork Poplar Creek—Current assessment and past trends* (p. 578). Oak Ridge National Laboratory. Retrieved from <https://info.ornl.gov/sites/publications/files/Pub70543.pdf>
- Brooks, S. C., & Southworth, G. R. (2011). History of mercury use and environmental contamination at the Oak Ridge Y-12 Plant. *Environmental Pollution*, *159*(1), 219–228. <https://doi.org/10.1016/j.envpol.2010.09.009>
- Brunner, P., Cook, P. G., & Simmons, C. T. (2009). Hydrogeologic controls on disconnection between surface water and groundwater: Hydrogeologic controls on the disconnect. *Water Resources Research*, *45*(1). <https://doi.org/10.1029/2008WR006953>
- Brunner, P., Cook, P. G., & Simmons, C. T. (2011). Disconnected surface water and groundwater: From theory to practice. *Ground Water*, *49*(4), 460–467. <https://doi.org/10.1111/j.1745-6584.2010.00752.x>
- Brunner, P., Therrien, R., Renard, P., Simmons, C. T., & Franssen, H.-J. H. (2017). Advances in understanding river-groundwater interactions: River-Groundwater Interactions. *Reviews of Geophysics*, *55*(3), 818–854. <https://doi.org/10.1002/2017RG000556>
- Cardenas, M. B., & Gooseff, M. N. (2008). Comparison of hyporheic exchange under covered and uncovered channels based on linked surface and groundwater flow simulations. *Water Resources Research*, *44*(3). <https://doi.org/10.1029/2007WR006506>
- Chow, R., Parker, B. L., Steelman, C. M., Thoms, A., & Nowak, W. (2021). How do fractures influence hyporheic exchange in sedimentary rock riverbeds? *Water Resources Research*, *57*(7). <https://doi.org/10.1029/2020WR028476>
- Clark, J. J., Qian, Q., Voller, V. R., & Stefan, H. G. (2019). Hyporheic exchange in a gravel bed flume with and without traveling surface waves. *Advances in Water Resources*, *123*, 120–133. <https://doi.org/10.1016/j.advwatres.2018.11.005>
- Crook, N., Binley, A., Knight, R., Robinson, D. A., Zarnetske, J., & Haggerty, R. (2008). Electrical resistivity imaging of the architecture of substream sediments. *Water Resources Research*, *44*(4). <https://doi.org/10.1029/2008WR006968>
- Cubbage, B., Noonan, G. E., & Rucker, D. F. (2017). A modified Wenner array for efficient use of eight-channel resistivity meters. *Pure and Applied Geophysics*, *174*(7), 2705–2718. <https://doi.org/10.1007/s00024-017-1535-9>
- Demers, J. D., Blum, J. D., Brooks, S. C., Donovan, P. M., Riscassi, A. L., Miller, C. L., et al. (2018). Hg isotopes reveal in-stream processing and legacy inputs in East Fork Poplar Creek, Oak Ridge, Tennessee, USA. *Environmental Sciences: Processes & Impacts*, *20*(4), 686–707. <https://doi.org/10.1039/C7EM00538E>
- Dey, A., & Morrison, H. F. (1979). Resistivity modelling for arbitrarily shaped two-dimensional structures. *Geophysical Prospecting*, *27*(1), 106–136. <https://doi.org/10.1111/j.1365-2478.1979.tb00961.x>
- Dong, W., Liang, L., Brooks, S., Southworth, G., & Gu, B. (2010). Roles of dissolved organic matter in the speciation of mercury and methylmercury in a contaminated ecosystem in Oak Ridge, Tennessee. *Environmental Chemistry*, *7*(1), 94. <https://doi.org/10.1071/EN09091>
- Fernandez, P. M., Bloem, E., Binley, A., Philippe, R. S. B. A., & French, H. K. (2019). Monitoring redox sensitive conditions at the ground-water interface using electrical resistivity and self-potential. *Journal of Contaminant Hydrology*, *226*, 103517. <https://doi.org/10.1016/j.jconhyd.2019.103517>
- Findlay, S. (1995). Importance of surface-subsurface exchange in stream ecosystems: The hyporheic zone. *Limnology & Oceanography*, *40*(1), 159–164. <https://doi.org/10.4319/lo.1995.40.1.0159>
- Hare, D. K., Briggs, M. A., Rosenberry, D. O., Boutt, D. F., & Lane, J. W. (2015). A comparison of thermal infrared to fiber-optic distributed temperature sensing for evaluation of groundwater discharge to surface water. *Journal of Hydrology*, *530*, 153–166. <https://doi.org/10.1016/j.jhydrol.2015.09.059>
- Harvey, J., & Gooseff, M. (2015). River corridor science: Hydrologic exchange and ecological consequences from bedforms to basins. *Water Resources Research*, *51*(9), 6893–6922. <https://doi.org/10.1002/2015WR017617>

- Ikard, S., Teeple, A., & Humberson, D. (2021). Gradient self-potential logging in the Rio Grande to identify gaining and losing reaches across the mesilla valley. *Water*, 13(10), 1331. <https://doi.org/10.3390/w13101331>
- Ikard, S. J., Briggs, M. A., & Lane, J. W. (2021). Investigation of scale-dependent groundwater/surface-water exchange in rivers by gradient self-potential logging: Numerical modeling and field experiments. *Journal of Environmental & Engineering Geophysics*, 26(2), 83–98. <https://doi.org/10.32389/JEEG20-066>
- Ikard, S. J., Carr, S. M., Terry, N. C., Briggs, M. A., & Payne, J. D. (2021). *Waterborne gradient self-potential, temperature, and conductivity logging of the upper Delaware river between Hancock and Port Jervis, New York, June–July 2021*. US Geological Survey Data Release. <https://doi.org/10.5066/P9H652Z8>
- Ikard, S. J., Rucker, D. F., Carroll, K. C., Adams, R. F., & Perez, G. M. (2022). Waterborne self-potential data, surface-water temperature and conductivity logging data, and electric resistivity tomography data measured at East Fork poplar creek, Oak Ridge, Tennessee, January–March 2022. [Dataset]. U.S. Geological Survey. <https://doi.org/10.5066/P9BAW75G>
- Ikard, S. J., & Sparks, D. D. (2020). *Waterborne gradient self-potential, temperature, and conductivity logging of lake Travis, Texas, near the Bee Creek Fault, March–April 2020*. U.S. Geological Survey Data Release. <https://doi.org/10.5066/P9CJDGN2>
- Ikard, S. J., Teeple, A. P., Payne, J. D., Stanton, G. P., & Banta, J. R. (2018). New insights on scale-dependent surface-groundwater exchange from a floating self-potential dipole. *Journal of Environmental & Engineering Geophysics*, 23(2), 261–287. <https://doi.org/10.2113/JEEG23.2.261>
- Kennedy, C. S. C. (2017). *Groundwater-surface water interactions in the discrete fracture networks of bedrock rivers (Doctoral dissertation)*. University of Guelph.
- Krause, S., Hannah, D. M., Fleckenstein, J. H., Heppell, C. M., Kaeser, D., Pickup, R., et al. (2011). Inter-disciplinary perspectives on processes in the hyporheic zone. *Ecohydrology*, 4(4), 481–499. <https://doi.org/10.1002/eco.176>
- Loar, J. M., Stewart, A. J., & Smith, J. G. (2011). Twenty-five years of ecological recovery of East Fork Poplar Creek: Review of environmental problems and remedial actions. *Environmental Management*, 47(6), 1010–1020. <https://doi.org/10.1007/s00267-011-9625-4>
- Loke, M. H., Acworth, I., & Dahlin, T. (2003). A comparison of smooth and blocky inversion methods in 2D electrical imaging surveys. *Exploration Geophysics*, 34(3), 182–187. <https://doi.org/10.1071/EG03182>
- Loke, M. H., Chambers, J. E., Rucker, D. F., Kuras, O., & Wilkinson, P. B. (2013). Recent developments in the direct-current geoelectrical imaging method. *Journal of Applied Geophysics*, 95, 135–156. <https://doi.org/10.1016/j.jappgeo.2013.02.017>
- Mamer, E. A., & Lowry, C. S. (2013). Locating and quantifying spatially distributed groundwater/surface water interactions using temperature signals with paired fiber-optic cables. *Water Resources Research*, 49(11), 7670–7680. <https://doi.org/10.1002/2013WR014235>
- McAliley, W. A., Day-Lewis, F. D., Rey, D., Briggs, M. A., Shapiro, A. M., & Werkema, D. (2022). Application of recursive estimation to heat tracing for groundwater/surface-water exchange. *Water Resources Research*, 58(6). <https://doi.org/10.1029/2021WR030443>
- McLachlan, P., Chambers, J., Uhlemann, S., Sorensen, J., & Binley, A. (2020). Electrical resistivity monitoring of river–groundwater interactions in a Chalk river and neighbouring riparian zone. *Near Surface Geophysics*, 18(4), 385–398. <https://doi.org/10.1002/nsg.12114>
- McLachlan, P. J., Chambers, J. E., Uhlemann, S. S., & Binley, A. (2017). Geophysical characterisation of the groundwater–surface water interface. *Advances in Water Resources*, 109, 302–319. <https://doi.org/10.1016/j.advwatres.2017.09.016>
- Meghdadi, A., & Javar, N. (2018). Evaluation of nitrate sources and the percent contribution of bacterial denitrification in hyporheic zone using isotope fractionation technique and multi-linear regression analysis. *Journal of Environmental Management*, 222, 54–65. <https://doi.org/10.1016/j.jenvman.2018.05.022>
- Mohamed, R. A. M., Brooks, S. C., Tsai, C.-H., Ahmed, T., Rucker, D. F., Ulery, A. L., et al. (2021). Geostatistical interpolation of streambed hydrologic attributes with addition of left censored data and anisotropy. *Journal of Hydrology*, 599, 126474. <https://doi.org/10.1016/j.jhydrol.2021.126474>
- Mohamed, R. A. M., Gabrielli, C., Selker, J. S., Selker, F., Brooks, S. C., Ahmed, T., & Carroll, K. C. (2021). Comparison of fiber-optic distributed temperature sensing and high-sensitivity sensor spatial surveying of stream temperature. *Journal of Hydrology*, 603, 127015. <https://doi.org/10.1016/j.jhydrol.2021.127015>
- Nyquist, J. E., & Corry, C. E. (2002). Self-potential: The ugly duckling of environmental geophysics. *The Leading Edge*, 21(5), 446–451. <https://doi.org/10.1190/1.1481251>
- Nyquist, J. E., Freyer, P. A., & Toran, L. (2008). Stream bottom resistivity tomography to map ground water discharge. *Ground Water*, 46(4), 561–569. <https://doi.org/10.1111/j.1745-6584.2008.00432.x>
- Oxtobee, J. P. A., & Novakowski, K. (2002). A field investigation of groundwater/surface water interaction in a fractured bedrock environment. *Journal of Hydrology*, 269(3–4), 169–193. [https://doi.org/10.1016/S0022-1694\(02\)00213-5](https://doi.org/10.1016/S0022-1694(02)00213-5)
- Oxtobee, J. P. A., & Novakowski, K. S. (2003). Ground water/surface water interaction in a fractured rock aquifer. *Ground Water*, 41(5), 667–681. <https://doi.org/10.1111/j.1745-6584.2003.tb02405.x>
- Peterson, M. J., Brooks, S. C., Mathews, T. J., Mayes, M. A., Johs, A., Watson, D. B., et al. (2018). Mercury remediation Technology development for lower east Fort Poplar Creek - FY2018 update (No. ORNL/SPR--2018/912, 1490603). <https://doi.org/10.2172/1490603>
- Rosenberry, D. O., Briggs, M. A., Delin, G., & Hare, D. K. (2016). Combined use of thermal methods and seepage meters to efficiently locate, quantify, and monitor focused groundwater discharge to a sand-bed stream. *Water Resources Research*, 52(6), 4486–4503. <https://doi.org/10.1002/2016WR018808>
- Rucker, D. F., Tsai, C.-H., Carroll, K. C., Brooks, S., Pierce, E. M., Ulery, A., & Derolph, C. (2021). Bedrock architecture, soil texture, and hyporheic zone characterization combining electrical resistivity and induced polarization imaging. *Journal of Applied Geophysics*, 188, 104306. <https://doi.org/10.1016/j.jappgeo.2021.104306>
- Ruppel, S. C., & Walker, K. R. (1984). Petrology and depositional history of a middle Ordovician carbonate platform: Chickamauga Group, Northeastern Tennessee, 95, 568–583. [https://doi.org/10.1130/0016-7606\(1984\)95%3C568:PADHOA%3E2.0.CO;2](https://doi.org/10.1130/0016-7606(1984)95%3C568:PADHOA%3E2.0.CO;2)
- Singha, K., Pidlisecky, A., Day-Lewis, F. D., & Gooseff, M. N. (2008). Electrical characterization of non-Fickian transport in groundwater and hyporheic systems. *Water Resources Research*, 44(4). <https://doi.org/10.1029/2008WR007048>
- Stegen, J. C., Johnson, T., Fredrickson, J. K., Wilkins, M. J., Konopka, A. E., Nelson, W. C., et al. (2018). Influences of organic carbon speciation on hyporheic corridor biogeochemistry and microbial ecology. *Nature Communications*, 9(1), 585. <https://doi.org/10.1038/s41467-018-02922-9>
- Tinkler, K., & Wohl, E. (1998). A primer on bedrock channels. In J. Tinkler & E. Wohl (Eds.), *Geophysical monograph series* (Vol. 107, pp. 1–18). American Geophysical Union. <https://doi.org/10.1029/GM107p0001>
- Trauth, N., Schmidt, C., Vieweg, M., Maier, U., & Fleckenstein, J. H. (2014). Hyporheic transport and biogeochemical reactions in pool-riffle systems under varying ambient groundwater flow conditions. *Journal of Geophysical Research: Biogeosciences*, 119(5), 910–928. <https://doi.org/10.1002/2013JG002586>
- Valois, R., Cousquer, Y., Schmutz, M., Pryet, A., Delbart, C., & Dupuy, A. (2018). Characterizing stream-aquifer exchanges with self-potential measurements. *Ground Water*, 56(3), 437–450. <https://doi.org/10.1111/gwat.12594>

- Ward, A. S., Gooseff, M. N., & Singha, K. (2010). Imaging hyporheic zone solute transport using electrical resistivity. *Hydrological Processes*, 24(7), 948–953. <https://doi.org/10.1002/hyp.7672>
- White, D. S. (1993). Perspectives on defining and delineating hyporheic zones. *Journal of the North American Benthological Society*, 12(1), 61–69. <https://doi.org/10.2307/1467686>
- Wroblicky, G. J., Campana, M. E., Valett, H. M., & Dahm, C. N. (1998). Seasonal variation in surface-subsurface water exchange and lateral hyporheic area of two stream-aquifer systems. *Water Resources Research*, 34(3), 317–328. <https://doi.org/10.1029/97WR03285>
- Zhody, A. A. R., Easton, G. P., & Mabey, D. R. (1974). *Application of surface geophysics to ground-water investigations (Techniques of Water-Resources Investigations No. 2* (p. 116). U.S. Geological Survey. Retrieved from <https://pubs.usgs.gov/twri/twri2-d1/html/pdf.html>